Peer-reviewed version available at *Robotics* **2019**, *8*, 65; doi:10.3390/robotics8030065

Article

Mechanical and Control Design of an Industrial Exoskeleton for Advanced Human Empowering in Heavy Parts Manipulation Tasks

Alessandro Mauri [1,2,†], Jacopo Lettori [1,3,‡], Giovanni Fusi [4], Davide Fausti [4], Maurizio Mor [4], Francesco Braghin [2], Giovanni Legnani [1,3], and Loris Roveda [1,5,‡*]

1 Consiglio Nazionale delle Ricerche (CNR), Istituto di Sistemi e Tecnologie Industriali per il Manifatturiero Avanzato (STIIMA), Milano, Italy
2 Politecnico di Milano, Department of Mechanical Engineering, Milano, Italy
3 University of Brescia, Department of Mechanical and Industrial Engineering, Brescia, Italy
4 Polibrixia, Brescia, Italy
5 Istituto Dalle Molle di Studi sull'Intelligenza Artificiale (IDSIA), Scuola Universitaria Professionale della Svizzera Italiana (SUPSI), Università della Svizzera Italiana (USI) IDSIA-SUPSI, Manno, Switzerland
* Correspondence: loris.roveda@idsia.ch
† First author

Abstract: Exoskeleton robots are a rising technology in industrial contexts to assist humans in onerous applications. Mechanical and control design solutions are intensively investigated to achieve a high performance human-robot collaboration (*e.g.*, transparency, ergonomics, safety, etc.). However, the most of the investigated solutions involve high-cost hardware, complex design solutions and standard actuation. In the presented work, an industrial exoskeleton for lifting and transportation of heavy parts is proposed. A low-cost mechanical design solution is proposed, exploiting compliant actuation at the shoulder joint to increase safety and transparency in human-robot cooperation. A hierarchic model-based controller is then proposed (including the modeling of the compliant actuator) to actively assist the human while executing the task. An inner optimal controller is proposed for trajectory tracking, while an outer fuzzy logic controller is proposed to online deform the task trajectory on the basis of the human's intention of motion. A gain scheduler is also designed to calculate the optimal control gains on the basis of the performed trajectory. Simulations have been performed in order to validate the performance of the proposed device, showing promising results. The prototype is under realization.

Keywords: Industrial exoskeleton design; industrial exoskeleton control; human-robot collaboration; optimal control; empowering fuzzy control.

1. Introduction

Exoskeletons are one of the key technologies to assist humans in a wide range of applications, such as rehabilitation, daily activities, etc. [1]. In particular, the adoption of exoskeletons in industrial applications is nowadays a *hot-topic* [2], since their capabilities to assist humans executing onerous tasks [3].

1.1. Industrial Exoskeletons: Design Solutions

Industrial exoskeletons can be classified as passive and active. Passive solutions are not provided by actuation, indeed, they use springs and/or dampers to store energy from human's motion and releasing it when required, such as [4]. The main advantages of these solutions are the reduced weight and size, do not requiring motors and batteries. However, commonly the mechanical design solutions are more complex. Moreover, active assistance cannot be generated, restricting the comfortable range of postures for the human worker.
Active exoskeletons are instead provided by actuation, allowing to empower the human worker. Different solutions have been developed in order to face different tasks, adopting different kinematics and hardware solutions. The *Panasonic Corporation* has developed an active device, called *AWN03*, that supports the operator's back when lifting heavy loads [5] thanks to electric motors. Another active human's back support has been

developed in [6]. *Stuttgart Exo-Jacket* has been developed in order to assist humans in industrial context, focusing on assembly tasks [7]. *HAL* exoskeleton developed by *Tsukaba University* [8] is a full body exoskeleton for medical and industrial applications. In [9] an under-actuated exoskeleton has been proposed to assist humans in industrial context. The proposed state-of-the-art solutions are still high-cost, characterized by a complex design and usually not involving compliant actuation (that can increase transparency, human-robot interaction performance and safety).

1.2. Industrial Exoskeletons: Control Solutions

Exoskeleton control is widely investigated in order to assist humans in different applications [10]. Many control approaches have been developed, integrating different sensors and control techniques. Brain-control schemes have been developed exploiting a electroencephalogram signals [11]. Surface electromyograpy measurements have been exploited in order to control the exoskeleton on the basis of the human's muscles activation [12], also exploiting variable impedance control [13]. Admittance force control has been also exploited in order to control the exoskeleton on the basis of the measured interaction between the human and the robot [14]. Common state-of-the-art approaches however show difficulties in the estimation of the human intention, especially while manipulating (partially) unknown payloads. Moreover, common approaches doesn't allow to online regulate the assistance given to the human during the task on the basis of the human-robot interaction.

1.3. Paper Contribution

The aim of this paper is to propose both the mechanical and control design of a low-cost exoskeleton (hardware costs $< 10000 Euro$) for industrial applications, involving compliant actuation to achieve transparency and intrinsic safety in human-robot interaction.
The target industrial application considered for the exoskeleton design specifications definition is a lifting and transportation task of a heavy component (as a case study a car bumper part, with weight of $10\,[kg]$). On the basis of such task, the kinematics of the exoskeleton has been defined, together with the performance required to the exoskeleton (*e.g.*, torques). A series elastic actuator (SEA) in the shoulder joint has been designed to embed compliance into the device. The SEA has been obtained by a compliant transmission (*i.e.*, a compliant belt) between the shoulder joint motor and the link. The target belt compliance has been calculated in order to achieve a specified equivalent shoulder joint compliance. On the basis of such specifications, components from the market (*e.g.*, motors, etc.) has been selected to implement the designed solution.
The proposed empowering controller has been designed in order to actively assist the human during the task execution, modulating the assistance on the basis of the human-robot interaction and being robust to (partially) unknown payloads. A hierarchic controller has been designed, composed by an inner optimal controller for task trajectory tracking and by an outer fuzzy logic controller for empowering the human, online modulating the assistance. The inner model-based controller includes the compliant modeling of the shoulder joint. The outer controller (on the basis of the proposed membership functions) is capable to identify the intention of motion of the human, reacting consequently. Moreover, a gain scheduler has been designed in order to store optimal control gains as a function of the performed task trajectory (*i.e.*, control gains are a function of the executed trajectory). Simulations studies have been performed in order to validate the proposed approach, simulating different task scenarios, showing promising results. The proposed exoskeleton is under realization.

2. Task Specifications & Exoskeleton's Design Guidelines

2.1. Task Description

The proposed exoskeleton has been designed considering a lifting task within the industrial context. The exoskeleton has to relieve the human from the lifting effort, while actively assisting him/her during the task. The reference task is, therefore, a bumper lifting task in a car assembly line (Figure 1 (a)). The adoption of the designed exoskeleton and of its control techniques can be extended to any heavy objects lifting task-like.
Considering the target part to be manipulated, the payload for the upper limbs exoskeleton is $P_e = 10\,[kg]$, *i.e.*, each arm has to lift (in ideal conditions) $P_a = 5[kg]$.

Considering the proposed application, two main positions will be assumed by the human wearing the exoskeleton during the task execution (Figure 1 (b)):

- **Configuration** 1: The arm is extended along the operator's trunk and the elbow position is 90° flexed;
- **Configuration** 2: The shoulder is flexed of 90° and the upper limb is completely extended. This is the most critical configuration considering the required motor torques.

It has been assumed that the task is composed of nine phases:

- *phase 0:* the operator positions the upper limbs in configuration 1 and the exoskeleton is turned on;
- *phase 1:* the operator positions the upper limbs without the external load, in order to grasp the object (configuration 1 in Figure 1);
- *phase 2:* the operator grasps the object (critical configuration 2 in Figure 1);
- *phase 3:* the operator moves back to configuration 1 carrying the part;
- *phase 4:* the operator transports the object maintaining upper limbs in configuration 1;
- *phase 5:* the operator lifts the external object up to configuration 2 to release the part in the final position;
- *phase 6:* the operator releases the object staying in configuration 2;
- *phase 7:* the operator moves back in configuration 1 without the part;
- *phase 8:* exoskeleton assistance is turned off.

2.2. Exoskeleton Specifications

In order to design the exoskeleton to face the proposed task, the following requirements have to be considered:

- kinematics;
- torques requirements;
- weight and size of the designed device;
- human safety and transparency requirements;
- economic affordability.

2.2.1. Kinematics

Considering the proposed task and its phases, the kinematics shown in Figure 2 has been proposed for the exoskeleton. In particular, the proposed kinematics is composed by 2 degrees of freedom (DoFs), allowing to perform the complete sequence of task phases while minimizing the DoFs of the device and, therefore, its complexity (*i.e.*, minimizing size, weight and cost of the solution). The *Denavit-Hartenberg paramters* of the this solution are summarized in Table 1.

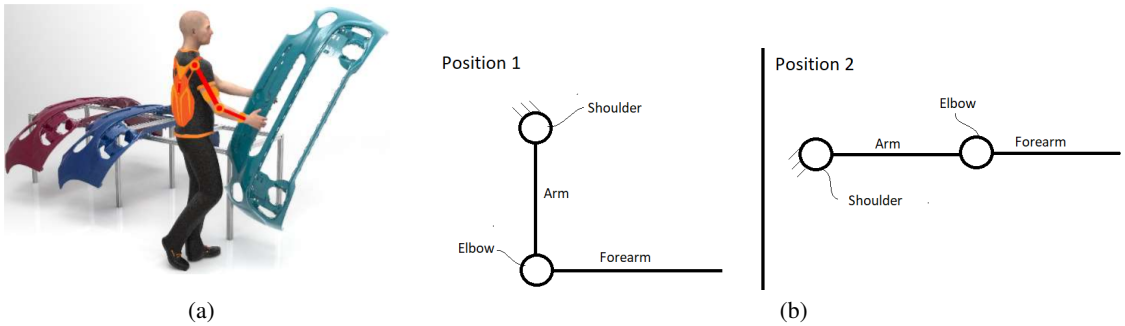

(a) (b)

Figure 1. (a) reference task: car bumper lifting and transportation. (b) human arm + exoskeleton configurations during task execution.

Table 1. Denavit Hartenberg parameters of the proposed device.

θ	α	r	d
θ_1	0	L_{linka}	0
θ_2	0	L_{linkf}	0

2.2.2. Torques Requirements

In order to define the torques requirements, the most critical configuration assumed by the exoskeleton during the task has to be considered. Therefore, configuration 2 will be used in order to calculate the required motor torques in order to compensate for the lifted load P_{load}, the human arm weight, composed by the human arm weight P_1 and by the human forearm and hand weight P_2, and to apply the required assistance to the human. The exoskeleton will, therefore, apply two forces on the upper limbs due to arm support and forearm support, supporting and assisting the worker during the target task execution. These forces compensate the external torques applied by the load, therefore, having the human generating no torques.
Figure 3 shows the exoskeleton-upper limb model, highlighting all the acting forces/torques, where:

- R_a: interaction force between the forearm and the exoskeleton;
- R_b: interaction force between the arm and the exoskeleton;
- R_s: vertical reaction force of the shoulder;
- a_1: application point of the R_b force;
- a_2: application point of the R_a force;
- L_{arm}: human's arm length;
- L_{f+h}: human's forearm and hand;
- P_{link_2}: weight of the forearm exoskeleton link applied in the middle of the link;
- P_{motor_2}: weight of the elbow motor;
- P_{link_1}: weight of the arm link applied in the middle of the link;
- τ_B: torque of the elbow motor to support the joint;
- τ_{mot}: torque of the shoulder motor to support the joint;

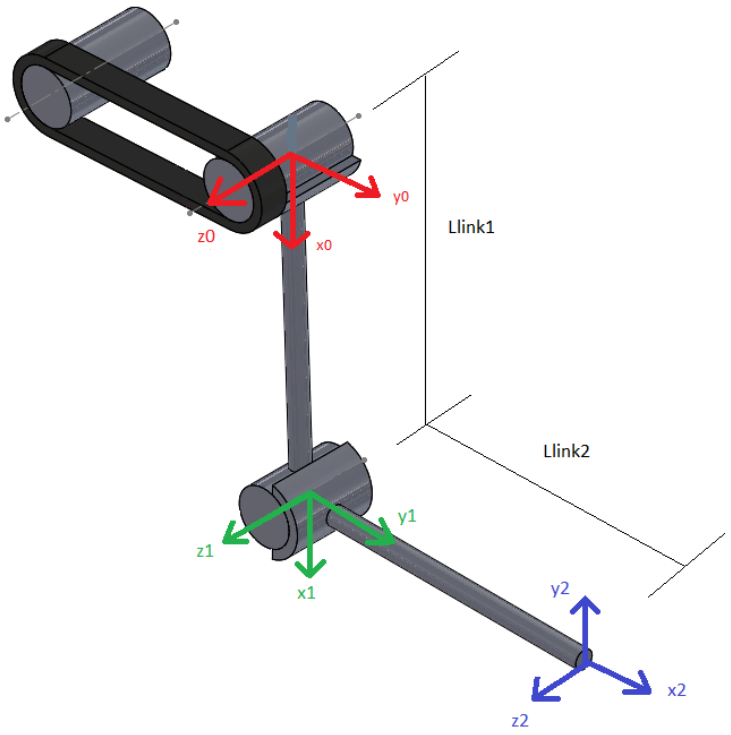

Figure 2. Kinematics of the proposed device.

Preprints (www.preprints.org) | NOT PEER-REVIEWED | Posted: 9 May 2019 doi:10.20944/preprints201905.0112.v1

Peer-reviewed version available at Robotics 2019, 8, 65; doi:10.3390/robotics8030065

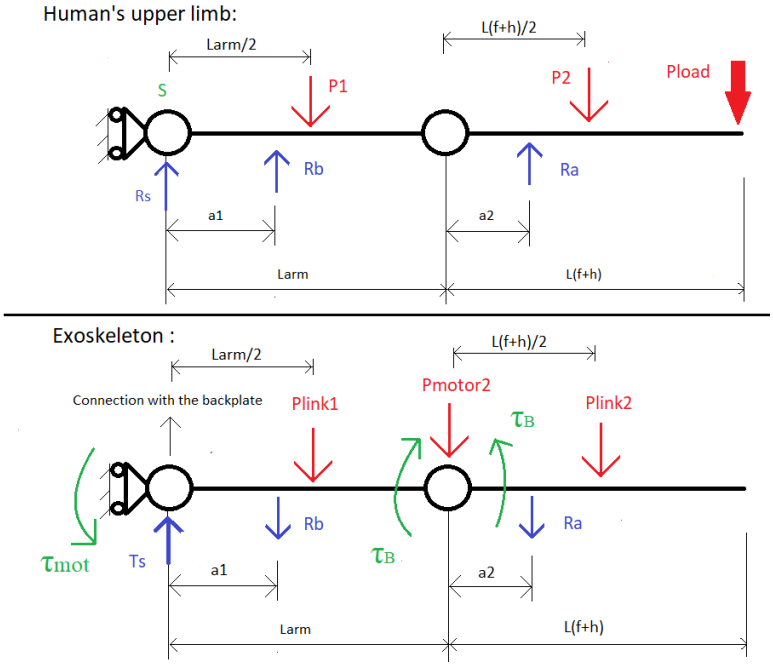

Figure 3. Loads acting on the exoskeleton in the critical configuration 2.

- T_s: vertical reaction force of the support connecting the exoskeleton link to the back-plate.

On the basis of [15] (detailing the average height of European adults) and on the basis of [16] (detailing the average weight of European adults), the following parameters have been chosen in order to define the human arm weight and length to be used in the above modeling:

- $Height = H = 180$cm.
- $Weight = W = 80$kg.

From these parameters it is therefore possible to calculate the modeling parameters from anthropometric tables [17]:

- $L_{arm} = 0.2898$m.
- $L_{forearm+hand} = 0.4536$m.
- $w_{arm} = 2.24$kg ($P_1 = 22$N).
- $w_{forearm+hand} = 1.76$kg ($P_2 = 17.27$N).

Assuming that (from a preliminary design) the weight of exoskeleton links is 0.5kg (*i.e.*, $P_{link_1} = P_{link_2} = 4.905\,[N]$), the weight of the elbow motor is 1kg ($P_{motor_2} = 9.81$N), $a_1 = \frac{L_{arm}}{2}$ and $a_2 = L_{f+h}$, it is possible to calculate reaction forces and the maximum static torques to be applied by the shoulder and elbow motors considering configuration 2 (Table 2). On the basis of such torques requirements, motors can be selected.

Table 2. Reaction forces and motor torques calculated to compensate for human arm weight and component weight in the critical configuration 2.

$R_a\ [N]$	$R_b\ [N]$	$T_s\ [N]$	$R_s\ [N]$	$\tau_{mot}\ [Nm]$	$\tau_B\ [Nm]$
57.68	39.29	116.56	−8.63	54.7	27.3

2.2.3. Weight and Size of the Designed Device

Considering that the upper limbs exoskeleton has to be transported by the human worker, its weight and size have to be reduced as much as possible. Therefore, the selection of the components (*e.g.*, motors) has to consider also such goal. Moreover, in order to limit the size of the designed device (in particular lateral dimension of the device) while ensuring the torques requirements, the shoulder motor has been positioned on the back support of the exoskeleton. Mechanical design of the links, etc., also considers both weight and size requirements.

Preprints (www.preprints.org) | NOT PEER-REVIEWED | Posted: 9 May 2019 doi:10.20944/preprints201905.0112.v1

Peer-reviewed version available at Robotics 2019, 8, 65; doi:10.3390/robotics8030065

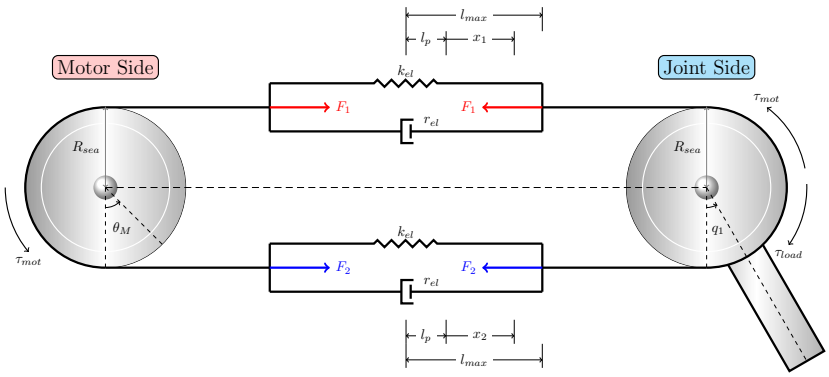

Figure 4. Mechanical model of the compliant belt shoulder joint actuation.

2.2.4. Human Safety and Transparency Requirements

In order to improve the transparency and the safety with respect to the human-robot collaboration, compliance has been embedded into the mechanical structure of the exoskeleton. In particular, a compliant transmission has been designed to connect the shoulder motor to the shoulder link. Such transmission has to be capable to produce an equivalent shoulder stiffness of $200[Nm/rad]$. Such equivalent stiffness is a medium-level value capable to give a degree of compliance to the exoskeleton while avoiding too high deformations.

2.2.5. Economic Affordability

In order to realize a low-cost device, components from the market have to be selected also satisfying the previous requirements. One of the main goal of the design is in fact to have hardware costs $< 10000 Euro$. Therefore, a balance between design specifications and hardware costs has to be found.

3. Exoskeleton Modeling & Design

3.1. Compliant Shoulder Joint Actuation Modeling

As mentioned in Section 2.2, the proposed exoskeleton design includes a compliant actuation for the shoulder joint. Such actuation system is composed by a compliant belt as a transmission between the motor and the shoulder joint. The concept of the compliant belt actuator is shown in Figure 4.
The aforementioned actuation system is modeled as the parallel of two mass-less spring-damper elements (with same stiffness k_{el} and damping r_{el} parameters). Being the radius of the pulleys both equal to $R_{sea} = 0.04[m]$, the deformation of each spring-damper element x_i are given by: $x_1 = -R_{sea}(q_1 - \theta_M)$ and $x_2 = R_{sea}(q_1 - \theta_M) = -x_1$.
In case of zero motor torque $\tau_{mot} = 0$, namely in the equilibrium position, the deformations are zero.
Overall torque transmission is given by the effect of pulling forces F_i on the two springs. Being l_{p_i} the pre-loaded lengths (equal for both springs), the forces are computed as $F_i = k_{el}(l_p + x_i) + r_{el}\dot{x}_i$. Therefore, the relation between motor torques and elastic belt deformations can be derived:

$$\tau_{mot} = -2R_{sea}^2 k_{el}(q_1 - \theta_M) - 2R_{sea}^2 r_{el}(\dot{q}_1 - \dot{\theta}_M) \tag{1}$$

3.2. Exoskeleton Dynamic Model

The overall mechanical system can be represented as a 3-DoFs system that moves in the sagittal plane, denoting with θ_M the shoulder motor joint position, with q_1 the shoulder joint position, with q_2 the exoskeleton elbow joint position. θ_M and q_1 are connected by the elastic belt, transmitting the torque by the relation (3.1). According to

Preprints (www.preprints.org) | NOT PEER-REVIEWED | Posted: 9 May 2019 doi:10.20944/preprints201905.0112.v1

Peer-reviewed version available at Robotics 2019, 8, 65; doi:10.3390/robotics8030065

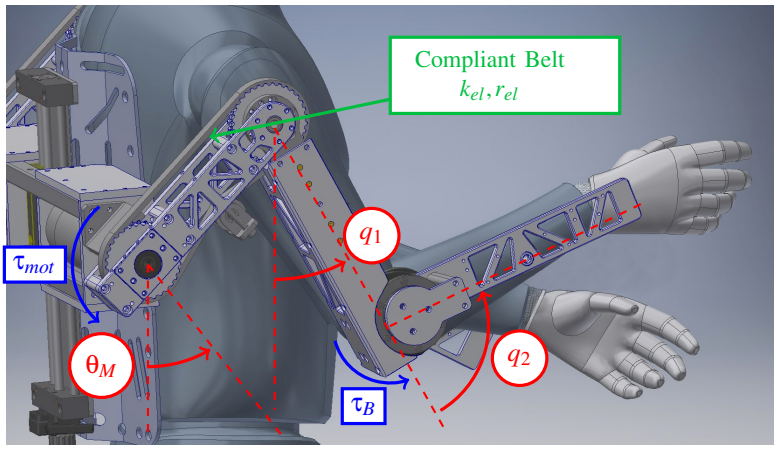

Figure 5. Elastic belt and joint torques are highlighted on the proposed exoskeleton model.

the *Euler-Lagrangian* formulation, the dynamics of the exoskeleton connected to the human arm can be expressed as follows:

$$\boldsymbol{M}(\boldsymbol{q})\ddot{\boldsymbol{q}} + \boldsymbol{C}(\boldsymbol{q},\dot{\boldsymbol{q}}) + \boldsymbol{G}(\boldsymbol{q}) + \boldsymbol{f}(\dot{\boldsymbol{q}}) + \boldsymbol{K}(\boldsymbol{q}) + \boldsymbol{D}(\dot{\boldsymbol{q}}) = \boldsymbol{\tau} - \boldsymbol{J}_e^T \boldsymbol{F}_e \tag{2}$$

where:

- $\boldsymbol{q} \in \boldsymbol{R}^{3x1}$ is the vector of DoFs $[\theta_M,\ q_1,\ q_2]^T$
- $\boldsymbol{M}(\boldsymbol{q}) \in \boldsymbol{R}^{3x3}$ is the system inertia matrix
- $\boldsymbol{C}(\boldsymbol{q},\dot{\boldsymbol{q}}) \in \boldsymbol{R}^{3x1}$ is the Coriolis and centrifugal vector
- $\boldsymbol{G}(\boldsymbol{q}) \in \boldsymbol{R}^{3x1}$ is the gravitational vector
- $\boldsymbol{f}(\boldsymbol{q},\dot{\boldsymbol{q}}) \in \boldsymbol{R}^{3x1}$ is the vector of friction forces
- $\boldsymbol{K}(\boldsymbol{q}) \in \boldsymbol{R}^{3x1}$ is the system elasticity vector
- $\boldsymbol{D}(\dot{\boldsymbol{q}}) \in \boldsymbol{R}^{3x1}$ is the system damping vector
- $\boldsymbol{\tau} \in \boldsymbol{R}^{3x1}$ is the vector of applied torques at the actuated joints
- $\boldsymbol{J}_e^T$ is the transposed extended Jacobian matrix
- $\boldsymbol{F}_e$ is the vector of external forces applied by the human and/or external load

The formulation in (2) represents three coupled second-order differential equations that relate the joint positions, velocities and accelerations to the joint torques $\boldsymbol{\tau} = [\tau_{mot},\ 0,\ \tau_B]^T$. In particular, τ_{mot} is the torque applied by the shoulder motor and τ_B is the torque applied by the elbow motor.
Combining the exoskeleton dynamics of the 2-DoFs manipulator with the compliant belt actuator in Section 3.1, it is possible to obtain the final overall 3-DoFs configuration. The resulting matrices comprehend terms coming both from the rigid mechanical system and the elastic coupling with the shoulder actuator. Angular velocities and positions of the shoulder joint q_1 and motor joint θ_M are coupled through the first two elements of the damping vector $\boldsymbol{D}(\dot{\boldsymbol{q}})$ and the stiffness vector $\boldsymbol{K}(\boldsymbol{q})$. The torque's transmission to the rigid system is explained in Section 3.1.
Figure 5 represents the CAD model of the exoskeleton and human arm, highlighting the joints (labeled in red), the actuation torques (in blue) and the compliant belt (green label).

3.3. Compliant Shoulder Joint Design

In order to select the elastic belt stiffness, a preliminary analysis have been performed considering the following stiffness values (peculiar for *off-the-shelves* elastic belts): $k_{el} = \{25000[N/m],\ 50000[N/m],\ 75000[N/m]\}$. Pre-load has also been varied from zero to the maximum pre-load force $F_{p_{max}} = k_{el}\frac{l_{max}}{2}$ (considering 5 values in such range). By increasing k_{el}, both the maximum transmittable torque and the equivalent shoulder joint stiffness increase (where the equivalent shoulder joint stiffness $K_{eq} = \frac{\partial \tau_{mot}}{\partial(q_1 - \theta_M)} = 2k_{el}R_{sea}^2$).
To select the elastic belt, a shoulder equivalent stiffness of $200[Nm/rad]$ has been imposed. Such equivalent stiffness is a medium-level value capable to give a degree of compliance to the exoskeleton while avoiding too

Preprints (www.preprints.org) | NOT PEER-REVIEWED | Posted: 9 May 2019 doi:10.20944/preprints201905.0112.v1

Peer-reviewed version available at Robotics 2019, 8, 65; doi:10.3390/robotics8030065

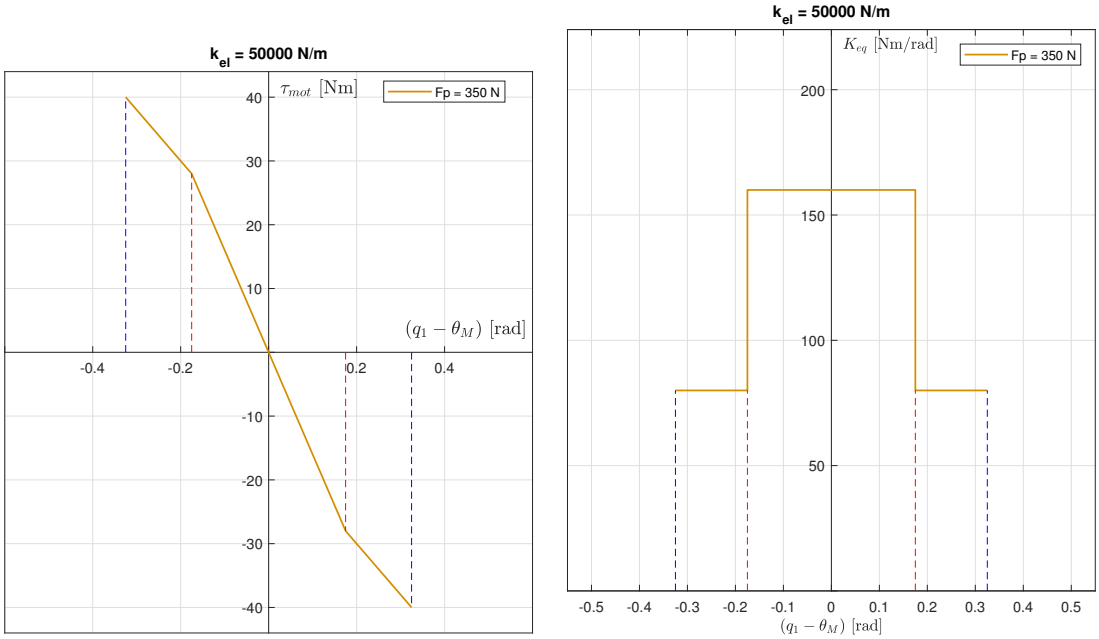

(a) (b)

Figure 6. (a) Stiffness characteristic of the chosen belt. (b) Equivalent stiffness at the link-side shoulder joint.

high deformations. k_{el} results then equal to $50000[N/m]$. Figure 6 (a) shows the stiffness characteristic curve and Figure 6 (b) the equivalent shoulder stiffness.

3.4. Design Solution

The 2 DoFs kinematics has been selected, with the *Denavit-Hartenberg paramters* in Table 1.
In order to satisfy the design specifications above described, the following components have been selected:

3.4.1. Brushless Motor Maxon EC60 FLAT/MILE/PM72

The Maxon motor *EC60 FLAT/MILE/PM72* (24V) has been selected as the shoulder motor, including:

- speed reducer IMS PM 72 C Ø72 mm, 4 stage, ratio 305 : 1.
- EC60 flat, brushless, with Hall sensors.
- encoder Maxon MILE, 1-1024 pulses, 3 differential channels.

The proposed motor satisfy the required static torque within its nominal torque and allows to apply higher pick torques for control purposes.

3.4.2. Transmission

The elastic belt *ELATECH* ® *SIT Spa* has been selected. The belt has a bielicoidal teeth with a progressive and continuous meshing in order to reduce vibrations and noises. 1 to 1 ratio (*EGLE*) pulleys have been selected.

3.4.3. Elbow actuator

robolink® *D High End robotic joint, size 20, symmetrical*, provided by *Igus* has been selected as the elbow actuator. This motor is composed by a stepper motor (NEMA17/23/23XL) which drives a revolute joint (code: RL-D-20-101-38-01033).

3.4.4. Exoskeleton CAD

Figure 7 shows the proposed exoskeleton. The thickness of the arm link is around 70mm and the elbow motor is positioned inside the link. The shoulder motor is fixed to the back-plate through an aluminium support. The

Preprints (www.preprints.org) | NOT PEER-REVIEWED | Posted: 9 May 2019 doi:10.20944/preprints201905.0112.v1

Peer-reviewed version available at Robotics 2019, 8, 65; doi:10.3390/robotics8030065

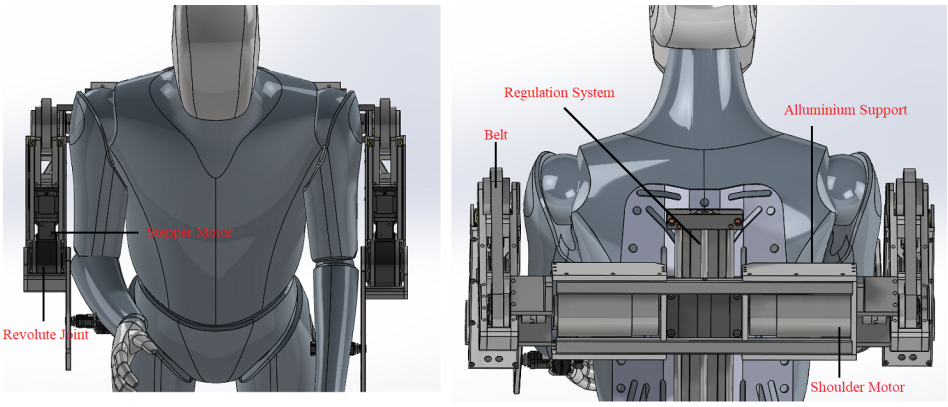

Figure 7. Exoskeleton prototype CAD model.

position of the support can be adjusted to increase the device wearability. The shoulder motor torque is transmitted to the human's shoulder through the compliant actuator. The link-side shoulder joint mounts an encoder in order to measure q_1 and, therefore, the angular deformation $q_1 - \theta_M$. On the basis of such measurement and on the basis of the elastic belt stiffness the external torque applied by the human/external load can be estimated and used in the control loop. The shoulder pulley has to be aligned with the shoulder axis parallel to the frontal plane in order to guarantee the flexion/extension degree of freedom. The elbow motor must be also aligned with the operator's elbow joint to guarantee the elbow rotation. The links length can be regulated in order to adapt the exoskeleton to the user.

4. Industrial Exoskeleton Control

4.1. Problem Formulation

The goal of the proposed controller is to assist the human in the lifting and transportation of heavy parts. To achieve such goal, the proposed control logic merges together the perks of the *optimal control* to obtain stability and robustness with the adaptability proposed by the *fuzzy logic*. A hierarchic controller has been designed, composed by an inner optimal control loop, to track a reference task trajectory, and by an outer fuzzy logic control loop, responsible for updating the commanded trajectory according to the detected intentions of motion of the human. The gain scheduling control allows to have online modification of the control gains of the inner optimal controller according to the commanded trajectory. The interaction torque τ_{int} between the human and the exoskeleton is calculated exploiting the encoders measurements at both the sides of the elastic belt elastic actuation. τ_{int} is exploited by the *fuzzy* controller in order to identify the intention of motion of the human.

4.2. Optimal Control Design

The inner *optimal control* guarantees the tracking and stabilization of the system around the task reference trajectory. Let the state-space form dynamic equations of a linear (or linearized) time-varying system be:

$$\begin{aligned} \dot{\boldsymbol{x}}(t) &= \boldsymbol{A}(t)\boldsymbol{x}(t) + \boldsymbol{B}(t)\boldsymbol{u}(t) \\ \boldsymbol{y}(t) &= \boldsymbol{C}(t)\boldsymbol{x}(t) \end{aligned} \tag{3}$$

where $\boldsymbol{x} \in \mathbb{R}^n$ is the state vector, $\boldsymbol{A}$ and $\boldsymbol{B}$ are the state and input matrix of the linearized system respectively, $\boldsymbol{u} \in \mathbb{R}^m$ is the control action vector and $\boldsymbol{y} \in \mathbb{R}^p$ is the output vector. According to the optimal control theory about *Linear Quadratic Regulator* ([18]), it is possible to define a quadratic cost function J as:

$$J = \frac{1}{2}\Delta\boldsymbol{x}^T(t_f)\boldsymbol{P}\Delta\boldsymbol{x}(t_f) + \frac{1}{2}\int_{t_0}^{t_f} \Delta\boldsymbol{x}^T\boldsymbol{Q}\Delta\boldsymbol{x} + \Delta\boldsymbol{u}^T\boldsymbol{R}\Delta\boldsymbol{u}\, dt \tag{4}$$

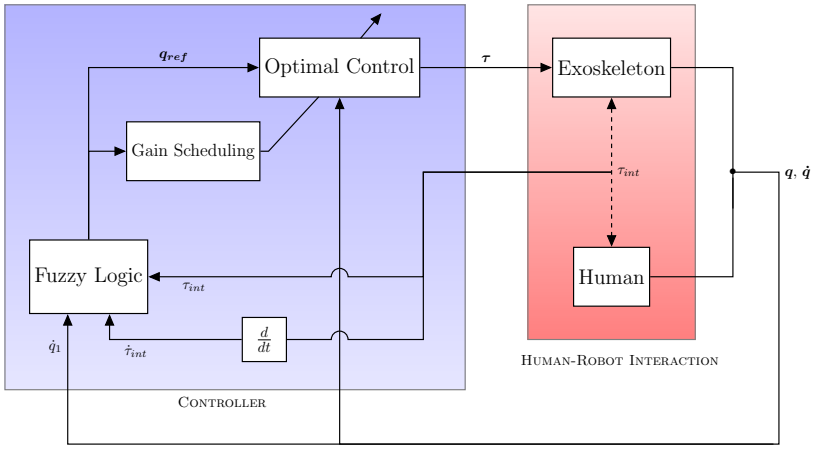

Figure 8. Overall control scheme showing the inner optimal controller, the outer fuzzy logic controller and the gain scheduler, highlighting the feedbacks to the control loops.

where $\Delta \boldsymbol{x} = \boldsymbol{q}_{ref} - \boldsymbol{q}$, $\boldsymbol{P}$ and $\boldsymbol{Q}$ are symmetric and positive semi-definite weight matrices and $\boldsymbol{R}$ is a symmetric and positive definite weight matrix. An optimal LQR controller can be designed in order to minimize this cost function, being the weight matrices previously defined.

4.3. Gain Scheduling Control Design

A *gain scheduling LQR* approach has been used in order to have a performing and stabilizing controller for all the possible configurations of the system. This offline controller, in fact, modifies the control gain matrix on the basis of the desired trajectory.

Basically, the nonlinear system outlined in Section 3 is quasi-linearized into several linear time-invariant (LTI) subsystems with respect to different operating points.

Let the nonlinear state equation of the system be represented as:

$$\dot{\boldsymbol{x}}(t) = f(\boldsymbol{x}(t), \boldsymbol{u}(t), t) = \left[\ddot{\theta}_M, \dot{\theta}_M, \ddot{q}_1, \dot{q}_1, \ddot{q}_2, \dot{q}_2\right]^T \tag{5}$$

The Taylor series expansion using the appropriate operating points $(\boldsymbol{x}^*, \boldsymbol{u}^*)$ can be obtained as $\dot{\boldsymbol{x}} = \boldsymbol{A}\boldsymbol{x} + \boldsymbol{B}\boldsymbol{u} + E_{rr}(\boldsymbol{x}^*, \boldsymbol{u}^*, t)$, where:

$$\boldsymbol{A} = \left.\frac{\partial f(\boldsymbol{x}, \boldsymbol{u})}{\partial \boldsymbol{x}}\right|_{\substack{\boldsymbol{x}=\boldsymbol{x}^* \\ \boldsymbol{u}=\boldsymbol{u}^*}} \quad \text{and} \quad \boldsymbol{B} = \left.\frac{\partial f(\boldsymbol{x}, \boldsymbol{u})}{\partial \boldsymbol{u}}\right|_{\substack{\boldsymbol{x}=\boldsymbol{x}^* \\ \boldsymbol{u}=\boldsymbol{u}^*}} \tag{6}$$

As demonstrated by [19], the system approximation error term $E_{rr}(\boldsymbol{x}^*, \boldsymbol{u}^*, t)$ can be neglected and this approach is to have the nonlinear system simply linearized as $\dot{\boldsymbol{x}} = \boldsymbol{A}\boldsymbol{x} + \boldsymbol{B}\boldsymbol{u}$.

Due to the fact that the linearization around the operating points holds, the plant and the weight matrices are assumed to be time-invariant and therefore t_f in the time interval can be assumed to be infinity.

If $\boldsymbol{P}(t)$ does converge, then for $t \ll t_f$, $\dot{\boldsymbol{P}} = 0$, the resulting equation for the LQR problem is the so-called *algebraic Riccati equation* (ARE):

$$0 = -\boldsymbol{Q} - \boldsymbol{P}\boldsymbol{A} - \boldsymbol{A}^T\boldsymbol{P} + \boldsymbol{P}\boldsymbol{B}\boldsymbol{R}^{-1}\boldsymbol{B}^T\boldsymbol{P} \tag{7}$$

Therefore if $\boldsymbol{P}_\infty$ exists, the corresponding steady-state feedback gain matrix is given by $\boldsymbol{K}_\infty = \boldsymbol{R}^{-1}\boldsymbol{B}^T\boldsymbol{P}_\infty$ and the resulting optimal control law is obtained as: $\Delta\boldsymbol{u}^*(t) = -\boldsymbol{K}\Delta\boldsymbol{x}(t)$.

The adopted strategy aims to apply the quasi-linearization approach to the several system configurations related to the typical arm lifting trajectory (letting q_1 vary from $0[^\circ]$ to $90[^\circ]$ and keeping the forearm perpendicular to

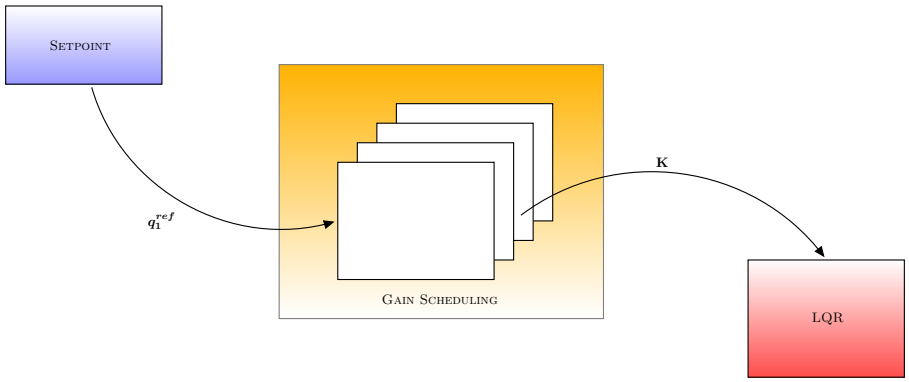

Figure 9. Gain schedule control gain matrix online update to the inner optimal controller.

the upper arm), computing the relative feedback control gains for each configuration and storing them for the following gain scheduling update, based on the reference set-point q_1^{ref}. The strategy is schematized in Figure 9.

4.4. Empowering Fuzzy Controller Design

The principal motivation to adopt a *fuzzy logic* for the outer human's intentions-based control is to deal with complex, ill-defined, uncertain and dynamic processes, which are intrinsically difficult to being modelled mathematically. In order to account for human behaviour inside the control architecture and establish more human-oriented input-output relations, a fuzzy table is built. The empowering fuzzy controller, therefore, is the highest level controller and it is responsible for the online modification of the reference trajectory, based on the human's intentions of motion.

The inputs of the developed fuzzy controller are the **interaction torque** τ_{int}, the **interaction torque derivative** $\dot{\tau}_{int}$, and **shoulder joint angular velocity** $\dot{q}_1$, while the output is the **assistance level** A_L that is yielded to the controller in order to modify the reference set-point of the optimal control.

The strategy behind the choice of the **inputs** membership functions is to obtain an adequate map of the general motion intentions from the human operator, classifying whether the applied torque is intentional or not, thus recognizing if the shoulder joint is willing to move from the current position or not. At the same time, an appropriate observance about safety between human and exoskeleton is achieved, by detecting if speed of the shoulder or interaction torque are too high with respect to a specified threshold. Moreover, the embedded strategy allows to recognize whether the human's intention is willing to lift (**lifting assistance**) or lower (**lowering assistance**) the arm, accordingly defining the deformation of the optimal control trajectory.

4.4.1. Membership Functions

The states of the membership function characterizing the shoulder joint velocity are: *stop*, *slow*, *move* and *fast*, whose aim is to decompose the velocity range into different states to know whether the shoulder angular variation is too fast in case of a possible unwanted movement or too slow or even still, in case the wearer does not want to change his/her arm position. The states of the membership function characterizing the interaction torque are: *N*, *S* and *NS*, which stand respectively for *no torque* (below a specified threshold the control is not activated), *safe* and *not safe*. Finally, the states of the membership function characterizing the interaction torque derivative are: *variation* (*V*) or *no variation* (*NV*), meaning if the operator wants to move the shoulder or change the motion by increasing or reducing the applied torque or not.

The **output** membership functions for the assistance level A_L range over four different fuzzy sets: *none*, *low*, *medium* and *high*.

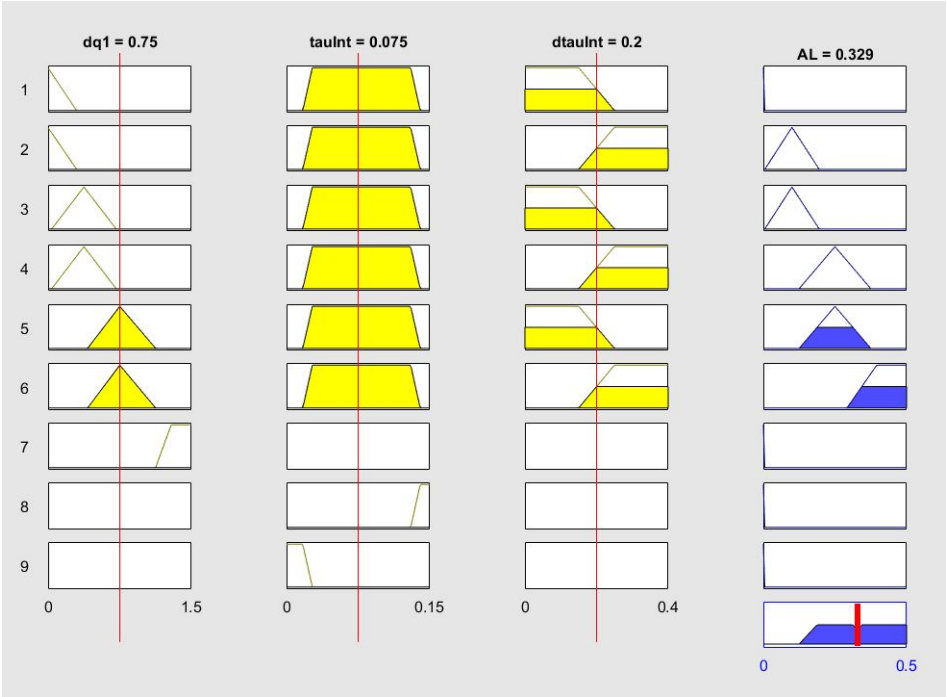

Figure 10. The nine fuzzy rules for the lifting assistance represented in MATLAB®.

4.4.2. Rule Base

The rule base for the current control strategy can be summed up with the following nine rules for the **lifting assistance** and eight rules for the **lowering assistance** (rule #8 is omitted for the lowering phase). The rule base adjusts the level of assistance depending on how much the operator is willing to move from the current arm position, respectively yielding null to high assistance to the shoulder motion:

$$\begin{cases} \#1 \quad \text{IF } \dot{q}_1 \text{ is } stop \text{ AND } \tau_{int} \text{ is } S \text{ AND } \dot{\tau}_{int} \text{ is } NV \text{ THEN } A_L \text{ is } none \\ \#2 \quad \text{IF } \dot{q}_1 \text{ is } stop \text{ AND } \tau_{int} \text{ is } S \text{ AND } \dot{\tau}_{int} \text{ is } V \text{ THEN } A_L \text{ is } low \\ \#3 \quad \text{IF } \dot{q}_1 \text{ is } slow \text{ AND } \tau_{int} \text{ is } S \text{ AND } \dot{\tau}_{int} \text{ is } NV \text{ THEN } A_L \text{ is } low \\ \#4 \quad \text{IF } \dot{q}_1 \text{ is } slow \text{ AND } \tau_{int} \text{ is } S \text{ AND } \dot{\tau}_{int} \text{ is } V \text{ THEN } A_L \text{ is } medium \\ \#5 \quad \text{IF } \dot{q}_1 \text{ is } move \text{ AND } \tau_{int} \text{ is } S \text{ AND } \dot{\tau}_{int} \text{ is } NV \text{ THEN } A_L \text{ is } medium \\ \#6 \quad \text{IF } \dot{q}_1 \text{ is } move \text{ AND } \tau_{int} \text{ is } S \text{ AND } \dot{\tau}_{int} \text{ is } V \text{ THEN } A_L \text{ is } high \\ \#7 \quad \text{IF } \dot{q}_1 \text{ is } fast \text{ THEN } A_L \text{ is } none \\ \#8 \quad \text{IF } \tau_{int} \text{ is } NS \text{ THEN } A_L \text{ is } none \\ \#9 \quad \text{IF } \tau_{int} \text{ is } N \text{ THEN } A_L \text{ is } none \end{cases}$$

Figure 10 shows the process of fuzzy rule base for the lifting assistance developed in MATLAB®.
The online trajectory generation to be provided to the inner optimal controller and gain scheduler is, therefore, deformed by the required assistance by the human:

$$q_1^{ref} = q_1 - A_L \text{sign}(\tau_{int}) \tag{8}$$

In particular, the shoulder reference angular position is computed from a stored value of q_1 that is updated with a frequency of $50[Hz]$, only if the value of assistance level is different from zero. The value $A_L \text{sign}(\tau_{int})$ allows to establish whether the reference set-point needs to be decreased or increased with respect to the previous value, by considering the sign of the interaction torque.

Remark 1. It has to be underlined that the only use of the force measurements cannot allow the fuzzy logic to identify an intention of motion of the human (the weight of the arm/payload affects this estimation). Including the velocity and the force derivative in the fuzzy controller can instead allow to understand if the human is intended to move the exoskeleton. In this case, in fact, it is possible to monitor the full interaction state between the human and the robot.

Remark 2. The proposed controller extends the work in [20] including improved fuzzy membership functions and rules, together with the proposed lower level gain scheduling optimal controller.

5. Simulation Validation

The effectiveness of the proposed control architecture has been validated in simulation. All the analyses have been carried out for system's nominal parameters (Section 2.2), affected by uncertainties, in order to take into account modeling errors (*e.g.*, unknown upper limb anthropometric characteristics, involuntary tremor, etc.). The simulations are performed using MATLAB®/Simulink.

5.1. Empowering Human in Lifting Task

The proposed controller has been tested in simulation assisting the operator in a lifting task of a $10\,[kg]$ part. In the proposed simulation the payload is grasped at time equal to $1\,[s]$. At time equal to $4.5\,[s]$ a torque is applied by the human shoulder to interact with the exoskeleton. Three interaction torque levels are simulated in Figure 11: $8\,[Nm]$, $12\,[Nm]$ and $16\,[Nm]$. On the basis of the designed controller, the first interaction torque level is not able to activate the fuzzy controller to assist the human, while the second and third interaction torque levels activate the assistance, deforming the set-point to the optimal controller until the torque decreases to zero. The proposed controller is therefore capable to distinguish from required assistance, empowering the human operator.

5.2. (Partially) Unknown Part Manipulation Task

Concerning the real industrial scenario where the operator lifts and carries an external weight (like a car's bumper, Section 2.1), the proposed exoskeleton control logic has to guarantee an adequate support to the arm even manipulating partially unknown weight parts. The here presented simulation evaluates the performance of the dynamic model-based controller for an unknown load-handling task scenario.
The simulation in Figure 12 shows the shoulder joint position time history when external weight of $4[kg]$ is applied on the exoskeleton (at time $t = 1[s]$). The proposed controller has been compared with a PID controller. The fuzzy logic controller identifies that such load application is not resulting from a human intention of motion, therefore, not updating the reference trajectory to the inner optimal controller and gain scheduler. Comparing the results with the PID controller, the proposed controller suppress the vibration while resulting in less deformation of the joint position.

6. Concept Mechanical Design of a 3 Degrees of Freedom Shoulder Joint

In order to improve the mobility of the shoulder joint, a 3 DoFs shoulder joint concept is here proposed, implementing 2 additional passive DoFs. In this new concept, the shoulder motor is considered aligned with the shoulder joint. The resulting exoskeleton implements therefore 4 DoFs (Figure 13).
The shoulder joint is composed by four links:

- $Link_1$: attached to the backplate;
- $Link_2$: its joint rotation guarantee the shoulder protraction/retraction degree of freedom;
- $Link_3$: it has to be aligned to the shoulder axis parallel to the sagittal plane. It guarantees the shoulder abduction/adduction degree of freedom;
- $Link_4$: its joint rotation allows the shoulder protraction/retraction. The final part is articulated with the arm link. It has to be aligned to the shoulder axis parallel to the frontal plane. The electric motor is be attached directly to the joint.

Peer-reviewed version available at Robotics 2019, 8, 65; doi:10.3390/robotics8030065

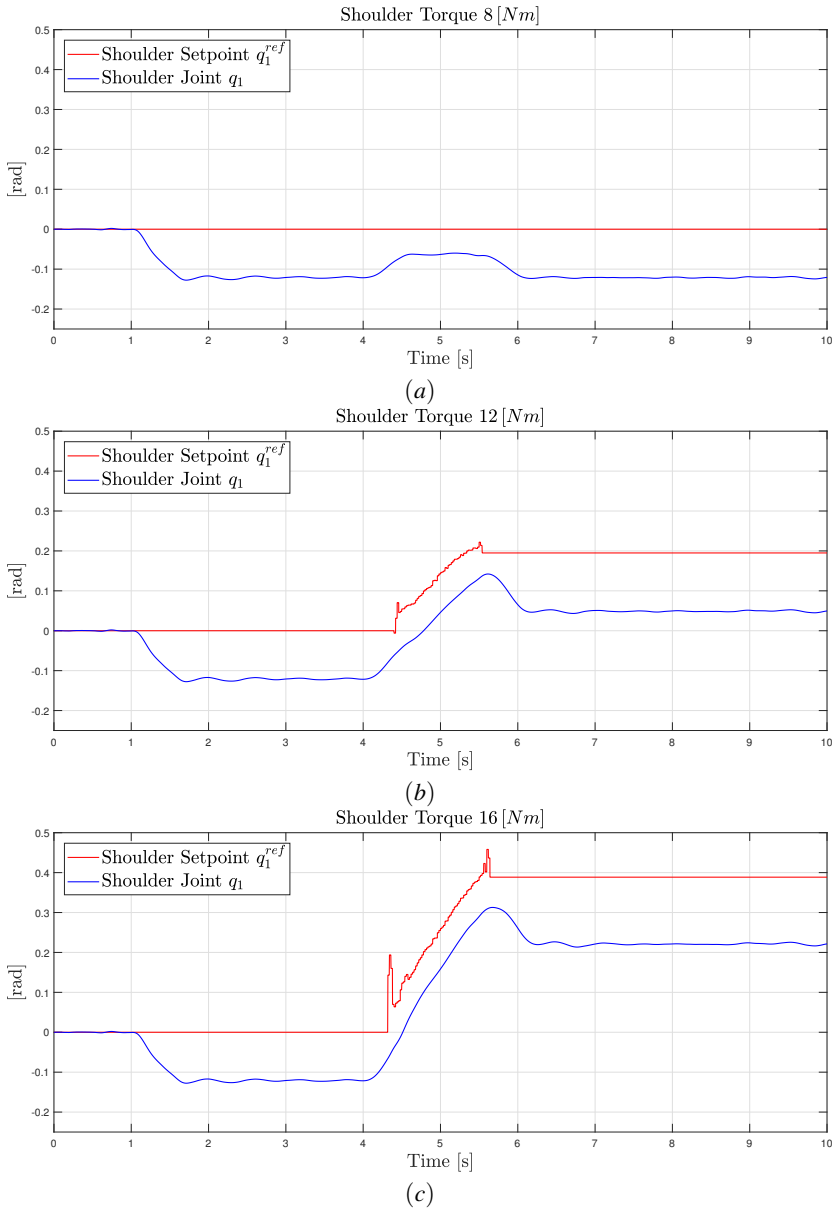

Figure 11. (a) the interaction torque level 8 $[Nm]$ is applied while manipulating the 10 $[kg]$ payload. The applied interaction torque is not able to activate the fuzzy controller to deform the set-point to the optimal control to assist the operator. (b) and (c) are related respectively to the 12 $[Nm]$ and 16 $[Nm]$ interaction torque levels. The fuzzy controller is activated, empowering the operator. In (c) the assistance is higher then in (b) due to the higher interaction torque level.

The $joint_1$ and $joint_2$ have both a mechanical limit, restricting the joint rotation of the $joint_2$ and $joint_3$. They would prevent user's dangerous positions during the object lifting. These limits are both adjustable, allowing to choose the level of the rotation restriction. They can totally block the rotation or leave it almost completely free. A fixed mechanical limit has been implemented for $Link_3$, enabling this joint to support gravity loads. Another fixed mechanical limit for $Link_4$ has been implemented, preventing parallels configuration between $Link_3$ joint and the shoulder motor. The $Link_4$ is adjustable in length. This regulation has been implemented to increase the exoskeleton wearability, adapting its configuration to different users.

The *Denavit-Hartenberg paramters* of the proposed solution are summarized in Table 3 (Figure 14). The shoulder joint designed with aluminum 2014-T6, and its total weight is around 1.2kg.

Preprints (www.preprints.org) | NOT PEER-REVIEWED | Posted: 9 May 2019 doi:10.20944/preprints201905.0112.v1

Peer-reviewed version available at Robotics 2019, 8, 65; doi:10.3390/robotics8030065

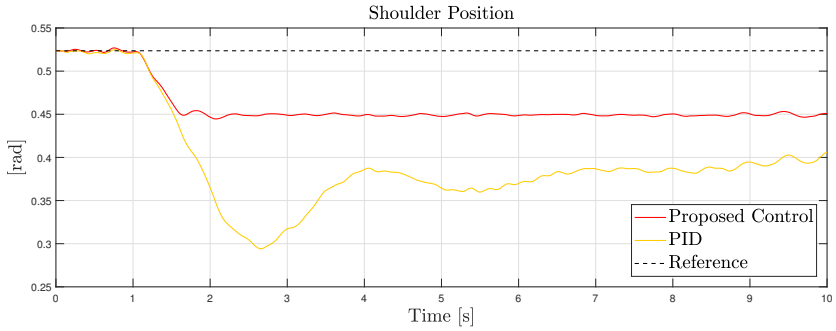

Figure 12. Comparison between the proposed controller and PID controller compensating a $4\,[kg]$ payload unknown weight. The proposed controller is capable to suppress vibration, resulting in less deformation.

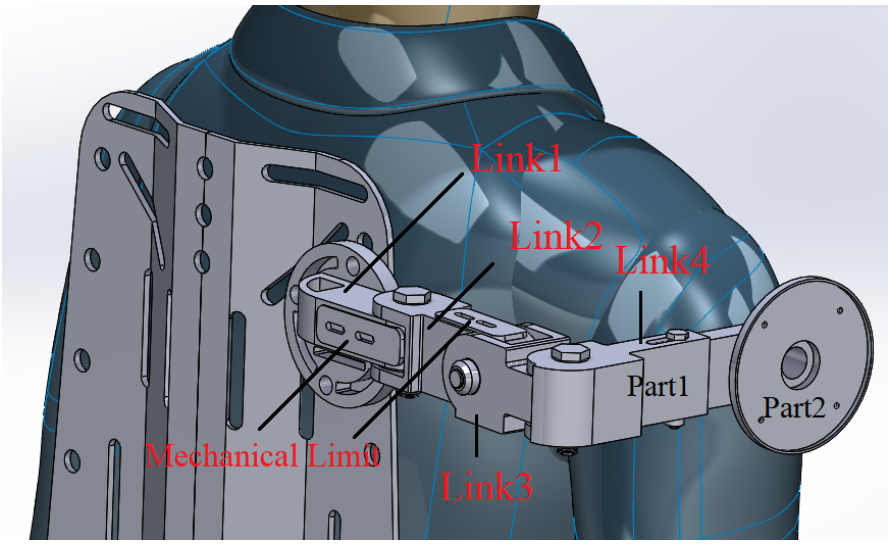

Figure 13. Three DoFs shoulder joint: new concept to increase exoskeleton mobility and task DoFs.

7. Conclusions

The here presented paper describes the mechanical and control design solutions for a hardware low-cost industrial exoskeleton to be adopted in lifting and transportation of heavy parts. Mechanical design specifications have been derived from the task, allowing to design an intrinsic compliant 2 DoFs exoskeleton. The proposed control architecture has been described, defining an inner gain scheduling optimal controller for task trajectory tracking and an outer fuzzy logic controller for human empowering. Simulation results show promising performance in the assistance of human operators (damping vibrations and empowering workers).

Current/future works are devoted to design a passive ergonomic back support for the exoskeleton, together to further investigate the 3 DoFs shoulder joint concept. Additionally, machine learning techniques are investigated to design the outer controller and to optimally tune its parameters.

The prototype of the proposed solution is under realization and it will be experimentally tested in the proposed task.

Table 3. Denavit-Hartenberg parameters of the exoskeleton implementing the new concept for the shoulder joint.

θ	α	r	d
θ_1	90	L_1	0
θ_2	-90	L_2	0
θ_3	90	L_3	0
θ_4	0	L_{Linka}	0
θ_5	0	L_{Linkf}	0

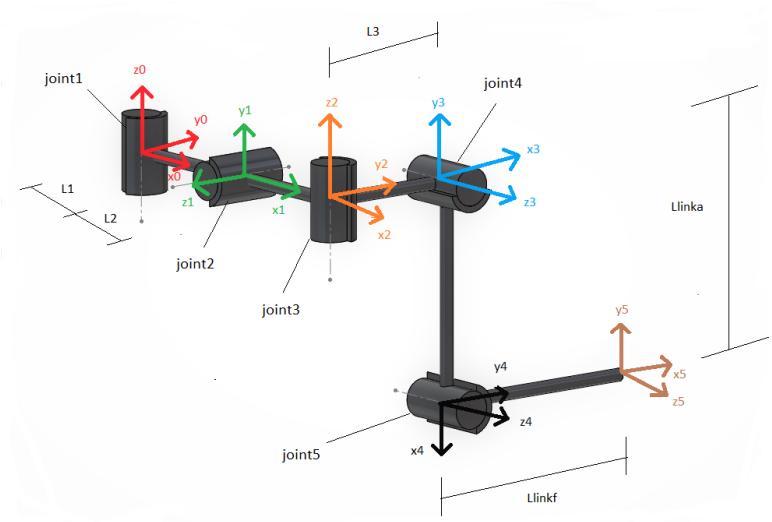

Figure 14. Kinematics of the new shoulder joint concept.

Acknowledgment

The work has been developed within the EFFORTLESS project, funded from CNR-STIIMA.
The work has been developed within the H2020 EUROBENCH STEPbySTEP project, funded from CNR-STIIMA.
Authors would like to thank Tito Dinon (CNR-STIIMA) for his expertise and support in the project.

1. Herr, H. Exoskeletons and orthoses: classification, design challenges and future directions. *Journal of neuroengineering and rehabilitation* **2009**, *6*, 21.
2. Bogue, R. Exoskeletons–a review of industrial applications. *Industrial Robot: An International Journal* **2018**, *45*, 585–590.
3. De Looze, M.P.; Bosch, T.; Krause, F.; Stadler, K.S.; O'Sullivan, L.W. Exoskeletons for industrial application and their potential effects on physical work load. *Ergonomics* **2016**, *59*, 671–681.
4. https://eksobionics.com/eksoworks/; Last visit in April 2019.
5. Li, R.Y.M.; Ng, D.P.L. Wearable Robotics, Industrial Robots and Construction Worker's Safety and Health. International Conference on Applied Human Factors and Ergonomics. Springer, 2017, pp. 31–36.
6. Huysamen, K.; de Looze, M.; Bosch, T.; Ortiz, J.; Toxiri, S.; O'Sullivan, L.W. Assessment of an active industrial exoskeleton to aid dynamic lifting and lowering manual handling tasks. *Applied ergonomics* **2018**, *68*, 125–131.
7. Ebrahimi, A. Stuttgart Exo-Jacket: An exoskeleton for industrial upper body applications. 2017 10th International Conference on Human System Interactions (HSI). IEEE, 2017, pp. 258–263.
8. Sankai, Y. HAL: Hybrid assistive limb based on cybernics. In *Robotics research*; Springer, 2010; pp. 25–34.
9. Stadler, K.S.; Altenburger, R.; Schmidhauser, E.; Scherly, D.; Ortiz, J.; Toxiri, S.; Mateos, L.; Masood, J. Robo-mate an exoskeleton for industrial use—concept and mechanical design. In *Advances in Cooperative Robotics*; World Scientific, 2017; pp. 806–813.
10. Anam, K.; Al-Jumaily, A.A. Active exoskeleton control systems: State of the art. *Procedia Engineering* **2012**, *41*, 988–994.
11. Noda, T.; Sugimoto, N.; Furukawa, J.; Sato, M.a.; Hyon, S.H.; Morimoto, J. Brain-controlled exoskeleton robot for BMI rehabilitation. 2012 12th IEEE-RAS International Conference on Humanoid Robots (Humanoids 2012). IEEE, 2012, pp. 21–27.
12. Li, Z.; Wang, B.; Sun, F.; Yang, C.; Xie, Q.; Zhang, W. sEMG-based joint force control for an upper-limb power-assist exoskeleton robot. *IEEE journal of biomedical and health informatics* **2014**, *18*, 1043–1050.
13. Li, Z.; Huang, Z.; He, W.; Su, C.Y. Adaptive impedance control for an upper limb robotic exoskeleton using biological signals. *IEEE Transactions on Industrial Electronics* **2017**, *64*, 1664–1674.

14. Yu, W.; Rosen, J.; Li, X. PID admittance control for an upper limb exoskeleton. Proceedings of the 2011 American control conference. IEEE, 2011, pp. 1124–1129.
15. Langtree, I. Height Chart of Men and Woman in Different Countries. *Canada: Disabled* **2018**.
16. Walpole, S.C.; Prieto-Merino, D.; Edwards, P.; Cleland, J.; Stevens, G.; Roberts, I. The weight of nations: an estimation of adult human biomass. *BMC public health* **2012**, *12*, 439.
17. Legnani, G.; Palmieri, G. *Fondamenti di meccanica e biomeccanica del movimento*; CittàStudi, 2016.
18. Lewis, F.L.; Vrabie, D.; Syrmos, V.L. *Optimal control*; John Wiley & Sons, 2012.
19. Tao, C.W.; Taur, J.S.; Chen, Y. Design of a parallel distributed fuzzy LQR controller for the twin rotor multi-input multi-output system. *Fuzzy Sets and Systems* **2010**, *161*, 2081–2103.
20. Roveda, L.; Haghshenas, S.; Prini, A.; Dinon, T.; Pedrocchi, N.; Braghin, F.; Tosatti, L.M. Fuzzy impedance control for enhancing capabilities of humans in onerous tasks execution. 2018 15th International Conference on Ubiquitous Robots (UR). IEEE, 2018, pp. 406–411.